



Cite this: DOI: 10.1039/c7tc01533j

Flapping viscosity probe that shows polarity-independent ratiometric fluorescence†

Ryota Kotani,^a Hikaru Sotome,^b Hajime Okajima,^c Soichi Yokoyama,^a Yumi Nakaike,^a Akihiro Kashiwagi,^d Chigusa Mori,^d Yuki Nakada,^d Shigehiro Yamaguchi,^d Atsuhiko Osuka,^a Akira Sakamoto,^{*c} Hiroshi Miyasaka^{*b} and Shohei Saito^{*ae}

A variety of fluorescent molecular viscosity probes have been widely used for mapping the local viscosity in cells and for monitoring the microenvironments in materials. However, their viscosity-sensing structural design still relies strongly on molecular rotors featuring intramolecular rotational dynamics. Here we report flapping molecules (FLAP) as a ratiometric viscosity-sensing fluorophore that shows polarity-independent dual fluorescence. Viscosity-sensing mechanism is based on a unique V-shaped-to-planar conformational change in the singlet excited state (S_1), in which the flexible motion of an eight-membered ring plays an important role. Fast conformational dynamics have been studied by time-resolved spectroscopies, and the viscochromic properties have been quantitatively analyzed. Application of FLAP to monitoring the curing process of epoxy resins has also been demonstrated, in which other typical environment-sensitive dyes did not work as a local viscosity probe.

Received 10th April 2017,
Accepted 10th May 2017

DOI: 10.1039/c7tc01533j

rsc.li/materials-c

Introduction

Viscosity imaging with designed fluorescent probes is a useful technique because it enables mapping of the local viscosity of heterogeneous media.^{1,2} Although the local viscosity estimated by using the molecular probes does not simply correspond to the bulk viscosity measured by viscometers and rheometers, these properties are significantly related in homogeneous solvents (particularly in Newtonian fluids).^{1,3} Mapping spatial heterogeneity is an important advantage for the molecular viscosity probe compared with those instruments.

Molecular rotors have long been recognized as representative viscosity probes.^{1–3} Since the dynamic internal rotation in S_1 is suppressed in highly viscous media, the fluorescence (FL)

intensity of fluorogenic molecular rotors increases. These fluorophores have been applied to the study of microenvironments in polymeric materials^{2,4} and cellular organelles.⁵ Later, quantitative measurement of the local viscosity was developed with the ratiometric FL technique,^{1,6–8} in which the local viscosity can be estimated based on the intensity ratio of two FL bands at different wavelengths. Recently, the FL lifetime imaging microscopy (FLIM) technique has also been an important alternative to quantitative viscosity analysis, in which the viscosity-dependent FL lifetime of probe molecules is measured for mapping the heterogeneity in cells and materials.^{8a,b,9} With these techniques, a variety of sophisticated molecular rotors that show viscosity-sensing FL with small polarity dependence¹⁰ are now applied to quantitative viscosity imaging, for example, CVJ (cyanovinyljulolidine)-based,⁶ BODIPY (boron-dipyrromethene)-based,^{1g,8b,9} and Cy (cyanine)-based^{8a,c,9d,e} probes (Fig. 1a). However, structural design of these viscosity probes still relies on molecular rotors featuring the intramolecular rotational dynamics in S_1 (including a bond twisting which leads to *trans-cis* photoisomerization).^{11–13} Here we report unique flapping fluorophores as a new series of viscosity probes that show polarity-independent ratiometric FL properties. Our molecular design is different from molecular rotors but based on the hybridization of a flexible eight-membered ring (cyclooctatetraene, COT) and rigid fluorescent aromatic wings (Fig. 1b),¹⁴ which we have given the trivial name FLAP (flexible and aromatic photofunctional systems).

FLAP takes a V-shaped conformation in the ground state, while it is expected to undergo conformational relaxation in S_1

^a Department of Chemistry, Graduate School of Science, Kyoto University, Kitashirakawa Oiwake, Sakyo, Kyoto 606-8502, Japan.
E-mail: s_saito@kuchem.kyoto-u.ac.jp

^b Division of Chemistry, Graduate School of Engineering Science, Osaka University, Toyonaka, Osaka 560-8531, Japan

^c Department of Chemistry and Biological Science, College of Science and Engineering, Aoyama Gakuin University, 5-10-1, Fuchinobe, Chuo, Sagami-hara, Kanagawa 252-5258, Japan

^d Department of Chemistry, Graduate School of Science, Nagoya University, Furo, Chikusa, Nagoya 464-8602, Japan

^e Japan Science and Technology Agency (JST), PRESTO, Kitashirakawa Oiwake, Sakyo, Kyoto 606-8502, Japan

† Electronic supplementary information (ESI) available: Experimental procedures, theoretical calculations, time-resolved spectroscopies are included. See DOI: 10.1039/c7tc01533j

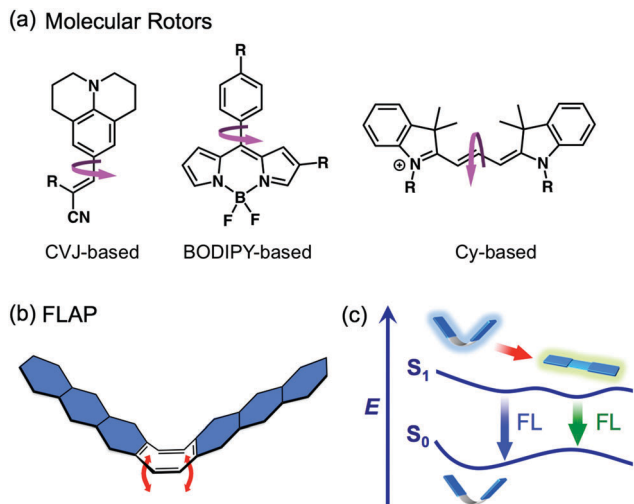


Fig. 1 Viscosity-sensing structural dynamics of (a) molecular rotors and (b) FLAP system. (c) Schematic energy diagram of FLAP.

to form a planar conformation (Fig. 1c). A unique feature of FLAP is possible dual FL from V-shaped and planar conformations. In this study, the importance of the COT flexibility in the dual FL mechanism has been demonstrated experimentally, and the photo-excited state dynamics of FLAP have been studied by time-resolved FL/IR spectroscopies as well as time-dependent density functional theory (TD-DFT) calculations. Polarity-independent ratiometric FL viscochromism of FLAP shows its efficacy in quantitative microviscosity analysis, and application to monitoring epoxy resin curing has also been demonstrated in comparison with other photo-responsive probes such as TICT (twisted intramolecular charge transfer)-type¹⁵ and ESIPT (excited-state intramolecular proton transfer)-type¹⁶ dyes.

Results and discussion

Synthesis

Scheme 1 outlines the synthetic route of a series of FLAP. This scheme was modified from the previously reported synthesis.¹⁴ A large-scale synthesis was prevented in the previous protocol because it included a photochemical rearrangement of 9,10-dihydro-9,10-ethenoanthracene¹⁷ to form a central eight-membered COT ring as a key step. In this photoreaction, the concentration of substrate solution had to be kept considerably low for efficient UV excitation, which hampered large-scale preparation. Instead, here we use Ni catalyzed [2+2+2+2] cycloaddition,¹⁸ reported by Wender & Christie, to form a COT core.

Precursor **4** (Scheme 1) was obtained in decagram scale by Diels–Alder reaction of 1,3-butadiene and dimethyl acetylenedicarboxylate, DDQ oxidation, and Wohl–Ziegler bromination. Introduction of TMS-ethynyl groups into **4** could not be achieved with TMS-ethynyl Grignard reagent and CuI.¹⁸ We presumed that the failure was due to undesirable side reactions at the ester groups, and thus attempted reaction of **4** with TMS-acetylene under milder reaction conditions (CuI, *n*-Bu₄NI and Cs₂CO₃),¹⁹ which led to successful TMS-ethynylation in 71% yield.

Subsequent deprotection of the TMS groups proceeded nicely upon treatment with AgNO₃²⁰ to afford **5** in 98% yield. Precursor **6** with a fused COT structure was obtained in gram scale in 51% yield from **5** using Ni catalyzed [2+2+2+2] cycloaddition¹⁸ and subsequent DDQ oxidation. Tetraester **6** was converted to tetraldehyde **9** by reduction with LiAlH₄ and subsequent Swern oxidation.

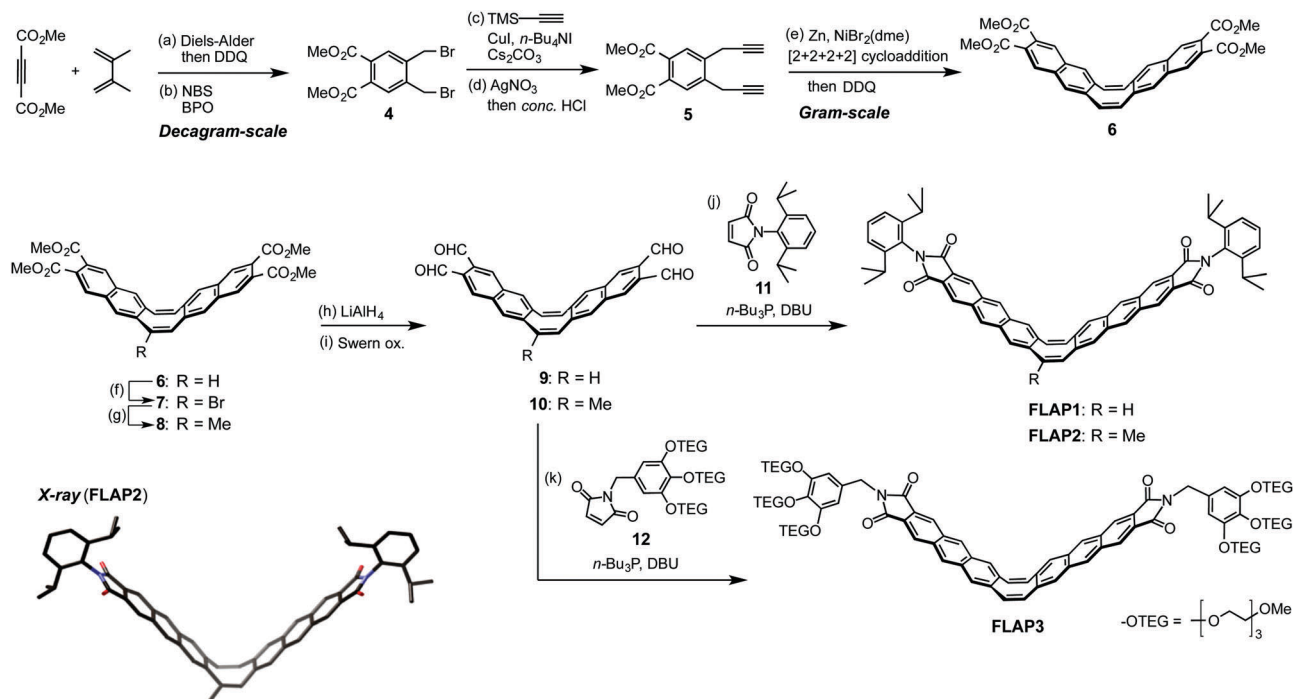
FLAP1, a standard model compound of the FLAP systems, was obtained from **9** with an acene-elongation reaction²¹ reported by Lin *et al.* To suppress strong aggregation,²² bulky substituents were introduced at the terminal maleimide groups in **FLAP1**. **FLAP2**, having a methyl group on the COT core, was synthesized in order to confirm an impact of conformational flexibility of the COT moiety on the FL properties. On the basis of the reported method,^{18b} mono-bromination of **6** and the subsequent methylation reaction were performed efficiently in 93% and 86% yields, respectively. Finally, hydrophilic **FLAP3** bearing six triethylene glycol groups was synthesized by the reaction of **9** with maleimide **12**. **FLAP3** was soluble in a mixed solvent system of DMSO/glycerol with a wide range of compositions, which have been commonly used media for quantitative evaluation of viscosity-independent properties.²³

Preliminary X-ray crystal structure determined that **FLAP2** had V-shaped geometry (Scheme 1, inset). The two anthracene-imide moieties were connected with two *cis*-olefins to form the tub-shaped COT ring. The torsion angle θ , defined by the neighboring carbon atoms C1, C2, C3, and C4 of the COT ring (Fig. 2, inset), was *ca.* 61 and 65°, in which the presence of the methyl group on the C3 or C8 carbon atom of the COT ring was crystallographically disordered. These torsion angles are comparable to those of the previously reported FLAP series ($\theta = 51\text{--}64^\circ$).^{14,22}

Steady-state fluorescence

Reflecting the structural similarity, the absorption spectra of **FLAP1** and **FLAP2** are almost the same, but the FL properties are remarkably different (Fig. 3). **FLAP1** showed intense green FL in tetrahydrofuran (THF) with peaks at 520, 561, and 607 nm and fluorescence quantum yield (Φ_f) of 0.34 (Fig. 3b, green line). The large Stokes shift (4580 cm⁻¹) of **FLAP1** suggested a large structural change in S_1 . Notably, a weak broad emission band was also observed in the blue region (450–500 nm) of the FL spectrum at room temperature. In the frozen glass of 2-methyl tetrahydrofuran (MTHF) medium at 77 K, the green emission band disappeared and the blue emission bands with vibronic peaks at 437, 467, and 494 nm increased in intensity (Fig. 3c).

In contrast, **FLAP2** exhibited blue FL in THF with peaks at 440 and 464 nm and $\Phi_f = 0.28$ (Fig. 3b, red line). The Stokes shift was 1200 cm⁻¹, much smaller than that of **FLAP1**, which indicated that the structural change of FLAP in S_1 was largely suppressed by introduction of only a methyl group onto the COT ring, and that the conformational flexibility of the COT ring was key in determining the dynamics of FLAP systems. At room temperature in MTHF, **FLAP2** showed similar absorption and FL spectra to those taken in THF. In MTHF matrix at 77 K,



however, the blue FL bands of **FLAP2** became sharper, and the maximum wavelengths were further blue-shifted to 435, 465, and 492 nm (Fig. 3d). This vibronic structure agreed well with that of **FLAP1** in the frozen medium, indicating that the structural change in *S*₁ of **FLAP2** was completely suppressed in the frozen medium, and the vibronic levels of the most stable *S*₀ geometry were reflected in the FL spectra at 77 K (see Fig. S1–S4, ESI† for further information of the steady-state fluorescence).

Calculated energy profile

Calculated energy profiles explained well the distinct FL properties of **FLAP1** and **FLAP2**. The corresponding FLAP structures **FLAP1'** and **FLAP2'** were used for the calculations, in which the terminal bulky substituents were replaced by hydrogen atoms (Fig. 2). The structural optimizations were performed using DFT for *S*₀ and TD-DFT for *S*₁ at the CAM-B3LYP/6-31+G(d) level.²⁴ The most stable geometries in *S*₀ were obtained with the V-shaped conformation ($\theta = 60.0^\circ$ for **FLAP1'** and $\theta = 66.4^\circ$ for **FLAP2'**), and the structural features were largely consistent with the X-ray crystal structures. In the optimized structures, owing to the bent conformation of the COT ring, the bond alternation around the *cis*-olefins was explicit and therefore the two anthraceneimide moieties were not efficiently π conjugated

(Fig. S5 and S6, ESI†). The *S*₀ energy profile was delineated using constrained DFT structural optimization with fixed COT dihedral angle θ (Fig. S7, ESI†). The *S*₀ energy became higher as the molecular shape came close to the flat form. Inversion behavior in *S*₀ between V- and Λ -shaped conformers was suggested for both **FLAP1** and **FLAP2**.

The *S*₁ energy profile was also described using TD-DFT constrained optimization with fixed θ from 0° to 80° at 5° intervals (Fig. 4). The *S*₁ profile of **FLAP1'** suggested that a shallow V-shaped structure and a planar one corresponded to different energy minima, and there was a small energy barrier between them. These energy-minimal structures were fully optimized as a shallow V-shaped conformation with $\theta = 54.5^\circ$ and the planar conformation with $\theta = 0^\circ$, and it is suggested that the planar form was slightly more stable (Fig. 4a).

On the basis of the calculated *S*₁ profile, the observed intense green FL at 520 nm of **FLAP1** was assigned to emission from the planar form, while the weak FL band observed in the blue region (450–500 nm) was assigned to emission from the shallow V-shaped form, respectively (Fig. 2). In the shallow V-shaped form, the electronic configuration arising from HOMO → LUMO transition was predominant in the *S*₁ electronic structure. These related orbitals were located on the anthraceneimide moieties

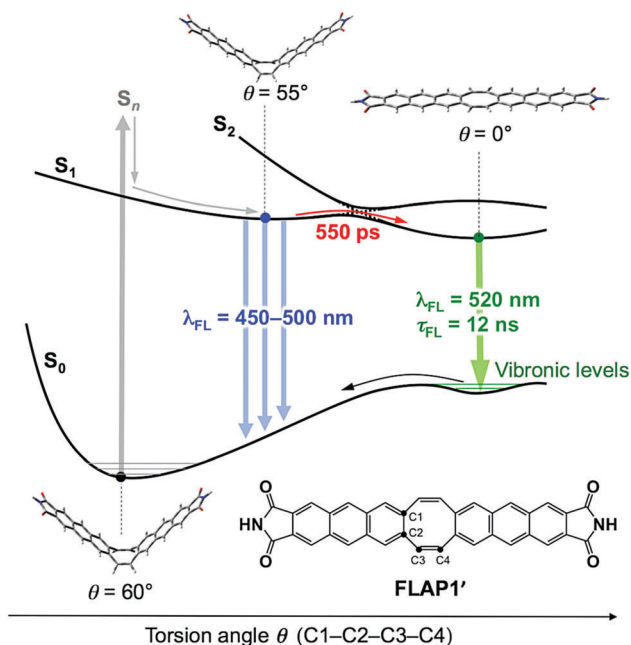


Fig. 2 Excited-state dynamics of **FLAP1**. The structural optimization of **FLAP1'** at the energy minimum points (a V-shaped form in S_0 , a shallow V-shaped form in S_1 , and a planar form in S_1) was performed using DFT for S_0 and TD-DFT for S_1 at the (CAM-)B3LYP/6-31+G(d) level.

without effective π conjugation through the COT joint (Fig. S8, ESI[†]). On approaching the flat conformation, π -orbital interaction on the COT ring became more significant, inducing a configurational change of S_1 that was responsible for the green FL. According to previous theoretical studies, the emissive planar form ($\theta = 0^\circ$) in S_1 has a trapezoid structure with C_{2v} symmetry (Fig. S9, ESI[†]) rather than a rectangle structure with D_{2h} symmetry (Fig. S10, ESI[†]).^{14b,25} The S_1 electronic structure of the C_{2v} planar form had contributions from the HOMO \rightarrow LUMO, HOMO-1 \rightarrow LUMO, HOMO \rightarrow LUMO+1 configurations, in which molecular orbitals delocalized over the entire π -conjugated frame were involved. The broad FL band observed in the blue region (450–500 nm) suggested the presence of multiple emissive points around the shallow V-shaped form. The observed clear vibronic bands in the green FL indicated that the vertical S_0 point of the green-emissive planar form was located near a local energy minimum in the S_0 energy surface (Fig. 2).

In sharp contrast, the calculated S_1 energy profile of **FLAP2'** afforded a single minimum with $\theta = 66.6^\circ$ (Fig. 4b and Fig. S11, S12, ESI[†]). The energy became increasingly higher upon decreasing θ value in S_1 , suggesting that the methyl group on the COT ring gave rise to steric hindrance for the conformational planarization in S_1 (as well as in S_0). The observed blue FL of **FLAP2** with smaller Stokes shift thus can be assigned to emission from the V-shaped structure.

It should be noted that the photochemical reactions reported for several COT derivatives²⁶ were not expected here, because the most probable photoinduced events of FLAP would be conformational changes rather than chemical reactions. The FL behavior of FLAP is rather similar to that of dibenzo[*b,f*]oxepin,²⁷

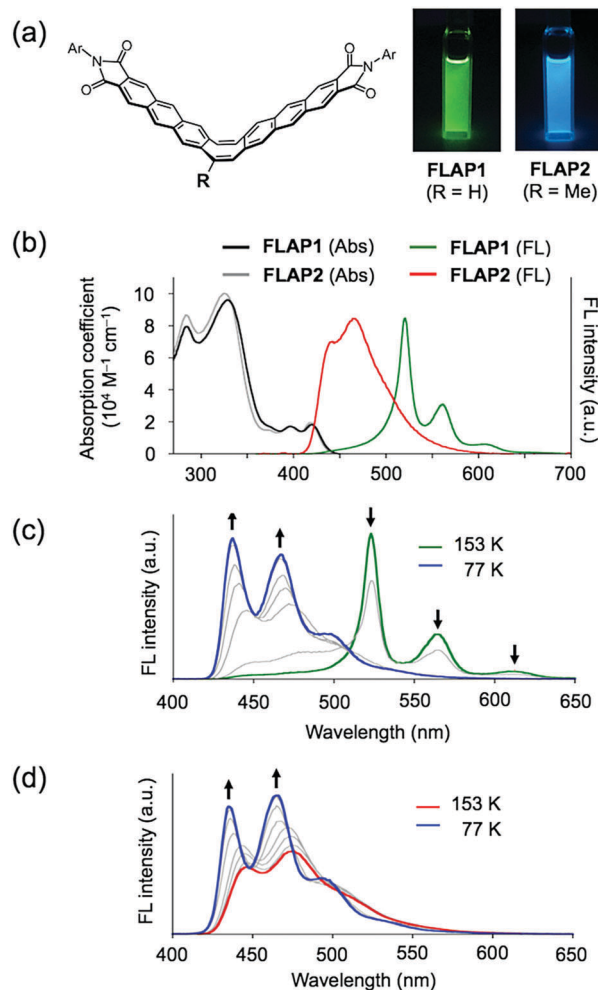


Fig. 3 (a) Fluorescence of **FLAP1** and **FLAP2** in THF under 365 nm UV lamp irradiation. Ar = 2,6-diisopropylphenyl. (b) Absorption and FL spectra of **FLAP1** and **FLAP2** in THF at room temperature. (c) Continuous change of the FL spectrum of **FLAP1** in MTHF during temperature decrease from 153 K to 77 K, and (d) that of **FLAP2**. Freezing point of MTHF is 137 K.

whose large Stokes shift has been explained by conformational planarization in S_1 originating from the excited-state 8 π aromaticity.²⁸

Time-resolved spectroscopy

To directly elucidate the conformational dynamics of FLAP in the excited state, we employed time-resolved FL and IR spectroscopies. Fig. 5 shows time-resolved FL spectra of **FLAP1** in DMSO solution excited with a 400 nm laser pulse. A broad emission band was observed around 450–500 nm immediately after the excitation. Since this broad emission appeared within the response time of the apparatus (*ca.* 40 ps), this emission band was attributed to the shallow V-shaped form. With an increase of the delay time after the excitation, this broad band gradually decreased with $\tau = 550$ ps, followed by the appearance of prominent bands around 530 and 570 nm. Then, the FL bands at 530 and 570 nm decayed with $\tau = 12.5$ ns.

The weak FL intensity around 450–500 nm still remained during the decay of the strong band at *ca.* 530 and 570 nm.

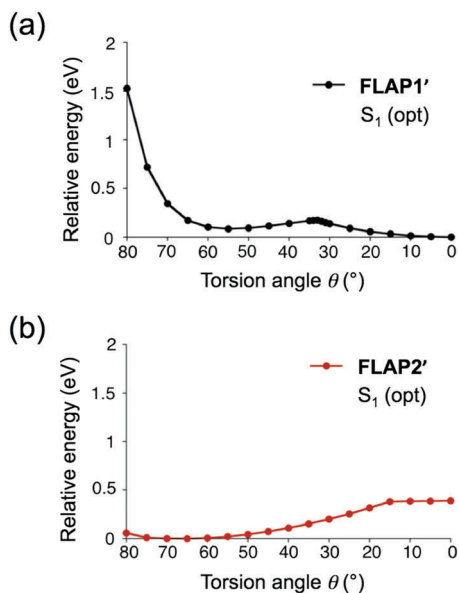


Fig. 4 S_1 energy profile of (a) **FLAP1'** and (b) **FLAP2'**. The constrained structural optimizations in S_1 were performed using TD-DFT at the CAM-B3LYP/6-31+G(d) level.

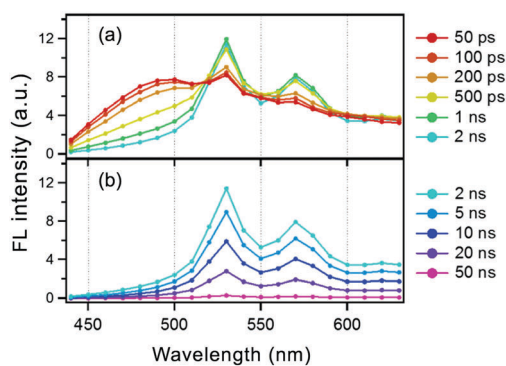


Fig. 5 Time-resolved FL spectra of **FLAP1** in DMSO, excited at 400 nm. (a) 50 ps–2 ns and (b) 2–50 ns.

Coexistence of these bands in the decay process indicated that the planar form was in equilibrium with the shallow V-shaped form. The presence of the multi-emissive points around the shallow V-shaped form in S_1 has been confirmed on the basis of the analysis of the FL time profiles in the wavelength range of 430–680 nm (Fig. S13, ESI[†]).

Time-resolved IR spectroscopy of **FLAP1** provided results consistent with the other analyses. In the wavenumber range of 1300–1400 cm^{-1} , well-resolved IR bands for each species were observed (Fig. 6a). Immediately after the excitation (2.5 ps), the ground-state bleaching at 1380 cm^{-1} was confirmed and, at the same time, the IR absorption band at 1353 cm^{-1} assignable to the shallow V-shaped form at the local minimum in S_1 was observed.

The IR band gradually shifted to the higher wavenumber side with a time constant of ~ 500 ps (Fig. S14, ESI[†]), which corresponds to the time constant measured by the time-resolved FL spectroscopy and is much longer than the vibrational cooling

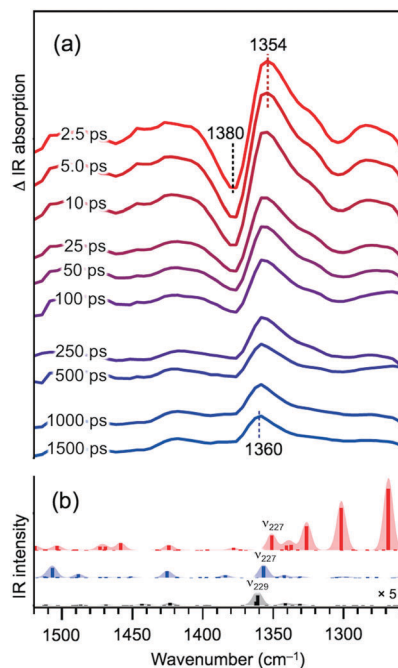


Fig. 6 (a) Time-resolved IR spectra of **FLAP1** in DMSO- d_6 , excited at 330 nm. (b) Calculated IR absorption bands of the shallow V-shaped form at the local minimum in S_1 (red bars), the planar form at the global minimum in S_1 (blue bars), and the most stable V-shaped form in S_0 (black bars) with a scaling factor of 0.98.

process. The IR band at 1358 cm^{-1} remained even after 1500 ps, at which time the conformational planarization in S_1 must be complete according to the time-resolved FL spectroscopy, and therefore this band was assigned to the planar form at the global minimum in S_1 . In comparison with the calculated IR absorption spectra of the respective optimized structures of **FLAP1** including bulky terminal substituents at the B3LYP/6-31G(d) level (Fig. 6b), these assignments were well supported; the observed bands at 1353, 1358, and 1380 cm^{-1} correspond to the ν_{227} of the shallow V-shaped form in S_1 , the ν_{227} of the planer C_{2v} trapezoid form in S_1 , and the ν_{229} of the V-shaped form in S_0 , respectively (Fig. 6b). All of them are C–N stretching vibrations between the terminal bulky substituents and the terminal imide moieties (Fig. S15, ESI[†]). Moreover, the calculated spectrum of S_1 (Fig. 6b) showed good agreements with the transient IR bands observed at 2.5–100 ps in the 1260–1330 cm^{-1} region attributed to the shallow V-shaped form in S_1 . As a consequence of these time-resolved spectroscopies, the excited-state dynamics of **FLAP1** in Fig. 2 were directly elucidated.

Polarity-independent viscochromism

Viscochromism of the FLAP system has been studied using the hydrophilic molecule **FLAP3** because **FLAP1** is not soluble in commonly used viscous media such as a mixed solvent of DMSO/glycerol.²³ This mixed solvent system is a well-studied Newtonian fluid, whose viscosity is constant regardless of the shear rate (namely, the rate of a rotating spindle on a viscometer). Polarity-independent FL properties were confirmed for

FLAP3 as well as **FLAP1**. As shown in Fig. 7a, the peak wavelength of the green emissive band showed a negligible shift within the 520–526 nm region in nonpolar to polar organic solvents such as toluene, tetrahydrofuran (THF), dichloromethane (DCM), dimethyl formamide (DMF), acetonitrile (MeCN), and dimethyl sulfoxide (DMSO). These solvents cover a wide range of relative dielectric constants ϵ_r from 2.4 to 46.7 at room temperature, while the viscosity values are within a small range of 0.4–2.2 cP. In spite of the wide range of relative dielectric constants, the spectral features of **FLAP3** were well preserved. The polarity independence suggested that the emissive structures in S_1 are not charge-polarized. The calculated μ^{ES} (excited-state dipole moments) and $\Delta\mu$ (the difference between excited state (ES) and ground state (GS) dipoles in the vertical geometry) of **FLAP1'** are 1.20 and 1.30 D for the planar C_{2v} trapezoid structure at the S_1 global minimum, while these values are 6.46 and 1.10 D, respectively, for the shallow V-shaped structure at the S_1 local minimum (Fig. S16, ESI†). These $\Delta\mu$ values (1.30 and 1.10 D) are significantly small, compared with the typical TICT systems having electron-donor and acceptor moieties.²⁹

On the other hand, **FLAP3** showed a remarkable viscosity dependence in FL (Fig. 7b). Simply by changing the volume ratio of DMSO/glycerol, mixed solvents having a wide range of

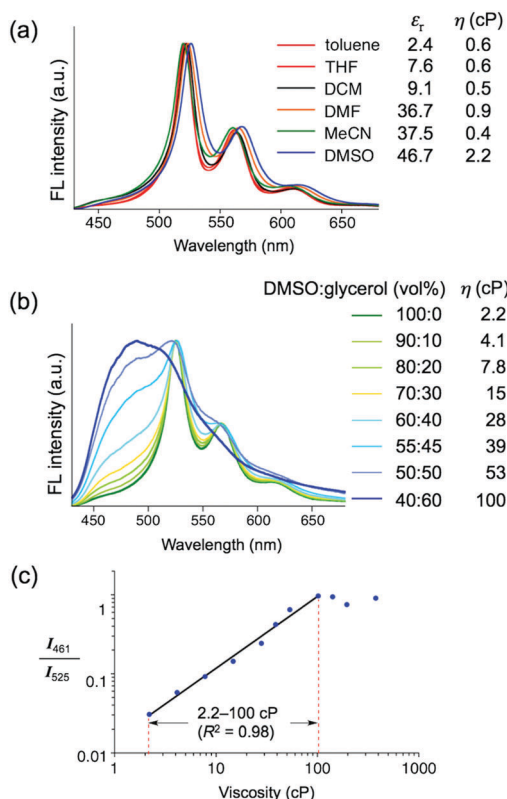


Fig. 7 Polarity-independent viscochromism of **FLAP3**. FL spectra (a) in common organic solvents and (b) in mixed solvents of DMSO/glycerol. Relative dielectric constants ϵ_r and viscosity η at room temperature are described as solvent indices. (c) Förster–Hoffmann equation plot. I_{461} and I_{525} describe the FL intensities at 461 and 525 nm, respectively.

viscosity were prepared. As the viscosity became higher, the relative intensity of the blue FL band (450–500 nm) gradually increased compared with the green FL band (525 nm). According to the Förster–Hoffmann equation,^{1,3d} the ratio of the FL intensities at 461 nm and 525 nm (I_{461}/I_{525}) was plotted *versus* viscosity measured at 25 °C in a double logarithmic graph (Fig. 7c). A linear relationship with a slope of 0.91 was observed in the viscosity range from 2.2 to 100 cP. In comparison with other reported viscosity probes,^{6–8} the viscosity-sensitive range is smaller, but the sensitivity in this range is remarkably high (Fig. S17, ESI†), which may originate from the different structural motion and the bulkier hydrophilic substituents of **FLAP3** compared with other molecular rotors. The polarity-independent ratiometric viscochromism of the FLAP fluorophore enables real-time visualization of local viscosity change without sensing the local polarity change.

Monitoring epoxy resin curing

The efficacy of FLAP as a polarity-independent viscosity probe was confirmed in the application to the real-time monitoring of epoxy resin curing.^{4e,g} Epoxy resin is a suitable platform for this purpose because both the local viscosity and polarity increase in the curing process. Reaction of epoxy groups with curing agents leads to generation of a number of polar hydroxy groups, while the microviscosity is expected to increase with the decrease of free volume. First, we used a prepolymer of bisphenol A diglycidyl ether **E1**, pentaerythritol tetrakis(2-mercaptoacetate) **H1**, and *n*-Bu₃N as epoxy agent, hardener, and catalytic accelerator, respectively (Fig. 8). This epoxy resin was cured in two steps: first, the epoxy prepolymer **E1** was mixed with the hardener **H1**, and second, a catalytic amount of *n*-Bu₃N was added to accelerate the cross-linking polymerization. In advance of the curing, a 0.1 wt% ratio of **FLAP1** was doped into **E1**. A fluid of **E1** doped with **FLAP1** showed green FL at 60 °C. After the addition of **H1** to **E1**, the green FL was still preserved at the same temperature, but the FL color turned into blue after the addition of *n*-Bu₃N, indicating the conformational planarization in S_1 of **FLAP1** was eventually suppressed.

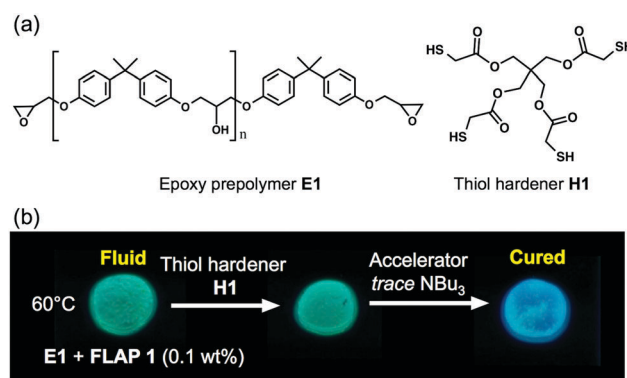


Fig. 8 (a) Chemical structures of epoxy prepolymer **E1** and thiol hardener **H1**. (b) Monitoring epoxy resin curing by using **FLAP1** as a molecular viscosity probe.

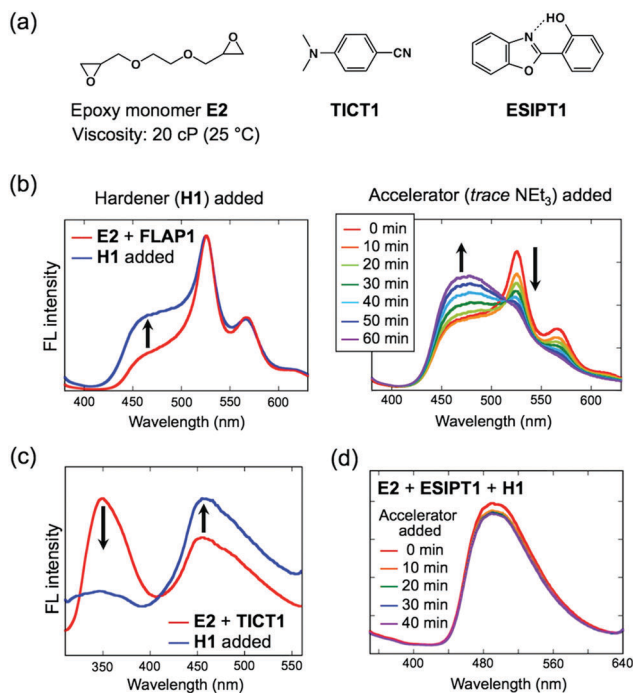


Fig. 9 (a) Chemical structures of the epoxy monomer **E2** and photoresponsive fluorophores **TICT1** and **ESIPT1**. Spectral change in the FL of (b) **FLAP1**, (c) **TICT1**, and (d) **ESIPT1** during the epoxy resin curing.

For quantitative evaluation, we selected ethylene glycol diglycidyl ether **E2** as epoxy monomer, whose viscosity is so low (20 cP) at 25 °C that the spectroscopic monitoring can be performed at room temperature (Fig. 9a). After the addition of **H1**, the I_{461}/I_{525} ratio of **FLAP1** changed from 0.22 to 0.50 (Fig. 9b, left), which corresponds to a local viscosity change from 20 to 49 cP according to the Förster-Hoffmann plot obtained above (Fig. 7c). Further addition of the *n*-Bu₃N accelerator induced a gradual spectral shift. In the curing process, the I_{461}/I_{525} ratio increased steadily and saturated at 1.30 (Fig. 9b, right). Although the estimated local viscosity was over the sensing limit (2.2–100 cP), the spectral analysis revealed that the curing process took 60 min after the addition of *n*-Bu₃N.

It should be noted here that, particularly in the case of non-Newtonian fluids such as concentrated polymer solutions, the local viscosity estimated by the chemical analysis must be regarded as a different index from the macroscopic viscosity measured by a physical method using a viscometer with a rotating spindle. The local viscosity, the so-called microviscosity, depends on the degree to which the excited-state structural change of photoresponsive fluorophores is suppressed. This should be closely related to the remaining free volume in condensed medium as well as the glass transition temperature.^{2,48} On the other hand, the macroscopic viscosity is defined from the physical aspect, namely the resistance to deformation of medium when a shear force is applied. The resistance mainly originates from the entanglement of polymer chains,³⁰ which is a different measure from the free volume remaining in the polymer matrix.

To compare the performance of **FLAP1** with those of other photoresponsive fluorophores, the same experiments were conducted using 4-dimethylaminobenzonitrile **TICT1** and

2-(2'-hydroxyphenyl)benzoxazole **ESIPT1** (Fig. 9a). These dyes are known for the typical behaviors of **TICT1**¹² and **ESIPT1**,¹³ respectively. Since **TICT1** has a more charge-polarized structure after the conformational change in *S*₁, the FL band with a large Stokes shift increased after the addition of the thiol hardener **H1** (Fig. 9c), which demonstrated **TICT1** did not work as a viscosity probe but rather as a polarity probe in the first curing step. In the case of **ESIPT1**, the FL band with a large Stokes shift was still observed even after the epoxy curing was completed (Fig. 9d). This result suggested that the structural change of the intramolecular proton transfer was too small to be suppressed by the external environmental change during the epoxy resin curing. These spectral tendencies of **TICT1** and **ESIPT1** were distinct from **FLAP1**, and the competence of the FLAP systems has been demonstrated as a polarity-independent ratiometric fluorescent probe.

Conclusions

In conclusion, flapping fluorophores (FLAP) have been explored as new viscosity probes with characteristic viscosity-sensing structural design, which is different from molecular rotors. FLAP displays polarity-independent ratiometric viscochromism as a single fluorophore, since the relative FL ratio of the V-shaped conformer versus the planar conformer depends on microviscosity and both the species are not charge-polarized. Fast conformational relaxation from the V-shaped to the planar conformation in the excited state of **FLAP1** has been revealed by time-resolved FL and IR analyses as well as theoretical calculations. The observed small Stokes shifts of **FLAP2** bearing a methyl group at the COT core indicated that even a small structural modification at the COT core has a large impact on its fluorescence. Polarity-independent viscochromism of **FLAP3** has been demonstrated in DMSO/glycerol mixed solvents, indicating that the flapping motion in the excited state does not involve an intramolecular charge transfer process. Quantitative viscosity evaluation has been realized with high sensitivity in the viscosity range of 2.2–100 cP. Finally, the competence of FLAP as a molecular viscosity probe has been indicated by monitoring epoxy resin curing with **FLAP1**. Improvement of the water solubility is currently underway for biochemical applications of the FLAP series.

Author contributions

R. K., S. Yokoyama, Y. N., A. K., C. M. and Y. N. performed the synthesis and the measurements of the steady-state absorption and FL. H. S. and H. M. conducted the time-resolved fluorescence spectroscopy. H. O. and A. S. performed the time-resolved IR spectroscopy. R. K., H. O., and S. S. performed the DFT and TD-DFT calculations. R. K., H. S., H. O. A. O., A. S. and S. S. co-wrote the manuscript, and S. Yamaguchi and H. M. proofread it. S. S. designed the FLAP molecules and directed the research project.

Acknowledgements

This work was supported by JST/PRESTO Grant Numbers JPMJPR12K5 and JPMJPR16P6 to S. S., by JSPS KAKENHI Grant

Numbers JP15H05482 and JP15H01083 to S. S., by JSPS KAKENHI Grant Numbers JP26107010 and JP16H00849 to A. S., and by JSPS KAKENHI Grant Number JP26107002 to H. M. The authors acknowledge Prof. Hideki Yorimitsu (Kyoto University) for the high resolution mass spectroscopy measurements, and thank Prof. Yuki Kurashige (Kyoto University) and Prof. Yoshikatsu Sato (ITbM, Nagoya University and ABiS) for fruitful discussion on the theoretical analysis and viscosity imaging, respectively.

Notes and references

- (a) M. A. Haidekker and E. A. Theodorakis, *J. Mater. Chem. C*, 2016, **4**, 2707–2718; (b) M. K. Kuimova, *Phys. Chem. Chem. Phys.*, 2012, **14**, 12671–12686; (c) M. A. Haidekker and E. A. Theodorakis, *Org. Biomol. Chem.*, 2007, **5**, 1669–1678; (d) A. S. Klymchenko, *Acc. Chem. Res.*, 2017, **50**, 366–375; (e) A. S. Klymchenko and R. Kreder, *Chem. Biol.*, 2014, **21**, 97–113; (f) Z. Yang, J. Cao, Y. He, J. H. Yang, T. Kim, X. Peng and J. S. Kim, *Chem. Soc. Rev.*, 2014, **43**, 4563–4601; (g) T. Kowada, H. Maeda and K. Kikuchi, *Chem. Soc. Rev.*, 2015, **44**, 4953–4972.
- (a) H. Itagaki, K. Horie and I. Mita, *Prog. Polym. Sci.*, 1990, **15**, 361–424; (b) B. Strehmel, V. Strehmel and M. Younes, *J. Polym. Sci., Part B: Polym. Phys.*, 1999, **37**, 1367–1386.
- (a) J. Stark and P. Lipp, *Z. Phys. Chem.*, 1913, **86**, 36–50; (b) G. C. Schmidt, *Ann. Phys.*, 1921, **65**, 247–256; (c) G. Oster and Y. Nishijima, *J. Am. Chem. Soc.*, 1956, **78**, 1581–1584; (d) T. Förster and G. Hoffmann, *Z. Phys. Chem.*, 1971, **75**, 63–69.
- (a) R. O. Loutfy, *Macromolecules*, 1981, **14**, 270–275; (b) R. O. Loutfy and B. A. Arnold, *J. Phys. Chem.*, 1982, **86**, 4205–4211; (c) R. O. Loutfy, *Macromolecules*, 1983, **16**, 678–680; (d) F. W. Wang, R. E. Lowry and B. M. Fanconi, *Polymer*, 1986, **27**, 1529–1532; (e) C. S. P. Sung and R. Mathisen, *Polymer*, 1987, **28**, 941–945; (f) J. Pączkowski and D. C. Neckers, *Macromolecules*, 1991, **24**, 3013–3016; (g) M. Younes, S. Wartewig, D. Lellinger, B. Strehmel and V. Strehmel, *Polymer*, 1994, **35**, 5269–5278; (h) D. Zhu, M. A. Haidekker, J.-S. Lee, Y.-Y. Won and J. C.-M. Lee, *Macromolecules*, 2007, **40**, 7730–7732; (i) K. P. Ghiggino, J. A. Hutchison, S. J. Langford, M. J. Latter, M. A. P. Lee, P. R. Lowenstern, C. Scholes, M. Takezaki and B. E. Wilman, *Adv. Funct. Mater.*, 2007, **17**, 805–813; (j) L.-L. Zhu, D.-H. Qu, D. Zhang, Z.-F. Chen, Q.-C. Wang and H. Tian, *Tetrahedron*, 2010, **66**, 1254–1260.
- (a) S. Lukac, *J. Am. Chem. Soc.*, 1984, **106**, 4386–4392; (b) C. E. Kung and J. K. Reed, *Biochemistry*, 1986, **25**, 6114–6121; (c) C. E. Kung and J. K. Reed, *Biochemistry*, 1989, **28**, 6678–6686; (d) T. Furuno, R. Isoda, K. Inagaki, T. Iwaki, M. Noji and M. Nakanishi, *Immunol. Lett.*, 1992, **33**, 285–288; (e) M. L. Viriot, M. C. Carre, C. Geoffroy-Chapotot, A. Brembilla, S. Muller and J. F. Stoltz, *Clin. Hemorheol. Microcirc.*, 1998, **19**, 151–160; (f) B. Wandelt, P. Cywinski, G. D. Darling and B. R. Stranix, *Biosens. Bioelectron.*, 2005, **20**, 1728–1736; (g) K. Yasuhara, Y. Sasaki and J. Kikuchi, *Colloids Surf., B*, 2008, **67**, 145; (h) M. E. Nipper, S. Majd, M. Mayer, J. C. M. Lee, E. A. Theodorakis and M. A. Haidekker, *Biochim. Biophys. Acta, Biomembr.*, 2008, **1778**, 1148–1153; (i) A. Hawe, V. Filipe and W. Jiskoot, *Pharm. Res.*, 2010, **27**, 314–326; (j) M. D. Molin, Q. Verolet, A. Colom, R. Letrun, E. Derivery, M. Gonzalez-Gaitan, E. Vauthey, A. Roux, N. Sakai and S. Matile, *J. Am. Chem. Soc.*, 2015, **137**, 568–571.
- (a) M. A. Haidekker, T. P. Brady, D. Lichlyter and E. A. Theodorakis, *J. Am. Chem. Soc.*, 2006, **128**, 398–399; (b) D. Fischer, E. A. Theodorakis and M. A. Haidekker, *Nat. Protoc.*, 2007, **2**, 227–236; (c) M. Dakanali, T. H. Do, A. Horn, A. Chongchivivat, T. Jarusreni, D. Lichlyter, G. Guizzunti, M. A. Haidekker and E. A. Theodorakis, *Bioorg. Med. Chem.*, 2012, **20**, 4443–4450.
- M. K. Kuimova, S. W. Botchway, A. W. Parker, M. Balaz, H. A. Collins, H. L. Anderson, K. Suhling and P. R. Ogilby, *Nat. Chem.*, 2009, **1**, 69–73.
- (a) X. Peng, Z. Yang, J. Wang, J. Fan, Y. He, F. Song, B. Wang, S. Sun, J. Qu, J. Qi and M. Yan, *J. Am. Chem. Soc.*, 2011, **133**, 6626–6635; (b) Z. Yang, Y. He, J.-H. Lee, N. Park, M. Suh, W.-S. Chae, J. Cao, X. Peng, H. Jung, C. Kang and J. S. Kim, *J. Am. Chem. Soc.*, 2013, **135**, 9181–9185; (c) F. Liu, T. Wu, J. Cao, S. Cui, Z. Yang, X. Qiang, S. Sun, F. Song, J. Fan, J. Wang and X. Peng, *Chem. – Eur. J.*, 2013, **19**, 1548–1553.
- (a) K. Suhling, L. M. Hirvonen, J. A. Levitt, P.-H. Chung, C. Tregidgo, A. L. Marois, D. A. Rusakov, K. Zheng, S. Ameer-Beg, A. Poland, S. Coelho, R. Henderson and N. Krstajic, *Med. Photonics*, 2015, **27**, 3–40; (b) M. K. Kuimova, G. Yahioglu, J. A. Levitt and K. Suhling, *J. Am. Chem. Soc.*, 2008, **130**, 6672–6673; (c) G. Hungerford, A. Allison, D. McLoskey, M. K. Kuimova, G. Yahioglu and K. Suhling, *J. Phys. Chem. B*, 2009, **113**, 12067–12074; (d) D. Fukushi, M. Kasuya, H. Sakuma and K. Kurihara, *Chem. Lett.*, 2011, **40**, 776–778; (e) E. Gatzogiannis, Z. Chen, L. Wei, R. Wombacher, Y.-T. Kao, G. Yefremov, V. W. Cornish and W. Min, *Chem. Commun.*, 2012, **48**, 8694–8696; (f) N. A. Hosny, G. Mohamedi, P. Rademeyer, J. Owen, Y. Wu, M.-X. Tang, R. J. Eckersley, E. Stride and M. K. Kuimova, *Proc. Natl. Acad. Sci. U. S. A.*, 2013, **110**, 9225–9230; (g) L. Wang, Y. Xiao, W. Tian and L. Deng, *J. Am. Chem. Soc.*, 2013, **135**, 2903–2906; (h) I. López-Duarte, T. T. Vu, M. A. Izquierdo, J. A. Bull and M. K. Kuimova, *Chem. Commun.*, 2014, **50**, 5282–5284; (i) N. A. Hosny, C. Fitzgerald, A. Vyšniauskas, A. Athanasiadis, T. Berkemeier, N. Uygur, U. Pöschl, M. Shiraiwa, M. Kalberer, F. D. Pope and M. K. Kuimova, *Chem. Sci.*, 2016, **7**, 1357–1367; (j) S.-C. Lee, J. Heo, J.-W. Ryu, C.-L. Lee, S. Kim, J.-S. Tae, B.-O. Rhee, S.-W. Kim and O. P. Kwon, *Chem. Commun.*, 2016, **52**, 13695–13698; (k) L. E. Shimolina, M. A. Izquierdo, I. López-Duarte, J. A. Bull, M. V. Shirmanova, L. G. Klapshina, E. V. Zagaynova and M. K. Kuimova, *Sci. Rep.*, 2017, **7**, 41097–41106.
- (a) M. A. Haidekker, T. P. Brady, D. Lichlyter and E. A. Theodorakis, *Bioorg. Chem.*, 2005, **33**, 415–425; (b) J. A. Levitt, P.-H. Chung, M. K. Kuimova, G. Yahioglu, Y. Wang, J. Qu and K. Suhling, *ChemPhysChem*, 2011, **12**, 662–672; (c) A. Filarowski, M. Kluba, K. Ciešlik-Boczula, A. Koll, A. Kochel, L. Pandey,

- W. M. De Borggraeve, M. Van der Auweraer, J. Catalán and N. Boens, *Photochem. Photobiol. Sci.*, 2010, **9**, 996–1008.
- 11 DCVJ Dynamics (a) B. D. Allen, A. C. Benniston, A. Harriman, S. A. Rostron and C. F. Yu, *Phys. Chem. Chem. Phys.*, 2005, **7**, 3035–3040; (b) C. Swalina and M. Maroncelli, *J. Phys. Chem. C*, 2010, **114**, 5602–5610; (c) S. Yang and K. Han, *J. Phys. Chem. A*, 2016, **120**, 4961–4965.
- 12 BODIPY Dynamics (a) L. Jiao, C. Yu, J. Wang, E. A. Briggs, N. A. Besley, D. Robinson, M. J. Ruedas-Rama, A. Orte, L. Crovetto, E. M. Talavera, J. M. Alvarez-Pez, M. Van der Auweraer and N. Boens, *RSC Adv.*, 2015, **5**, 89375–89388; (b) A. Prlj, A. Fabrizio and C. Corminboeuf, *Phys. Chem. Chem. Phys.*, 2016, **18**, 32668–32672.
- 13 Cyanine Dynamics (a) P. F. Aramendia, R. M. Negri and E. S. Roman, *J. Phys. Chem.*, 1994, **98**, 3165–3173; (b) M. E. Sanborn, B. K. Connolly, K. Gurunathan and M. Levitus, *J. Phys. Chem. B*, 2007, **111**, 11064–11074.
- 14 (a) C. Yuan, S. Saito, C. Camacho, S. Irle, I. Hisaki and S. Yamaguchi, *J. Am. Chem. Soc.*, 2013, **135**, 8842–8845; (b) C. Yuan, S. Saito, C. Camacho, T. Kowalczyk, S. Irle and S. Yamaguchi, *Chem. – Eur. J.*, 2014, **20**, 2193–2200.
- 15 (a) Z. R. Grabowski, K. Rotkiewicz and W. Rettig, *Chem. Rev.*, 2003, **103**, 3899–4031; (b) S. Sasaki, G. P. C. Drummen and G. Konishi, *J. Mater. Chem. C*, 2016, **4**, 2731–2743; (c) S. Sasaki, S. Suzuki, W. M. C. Sameera, K. Igawa, K. Morokuma and G. Konishi, *J. Am. Chem. Soc.*, 2016, **138**, 8194–8206.
- 16 (a) J. E. Kwon and S. Y. Park, *Adv. Mater.*, 2011, **23**, 3615–3642; (b) V. S. Padalkar and S. Seki, *Chem. Soc. Rev.*, 2016, **45**, 169–202.
- 17 P. W. Rabideau, J. B. Hamilton and L. Friedman, *J. Am. Chem. Soc.*, 1968, **90**, 4465–4466.
- 18 (a) P. A. Wender and J. P. Christy, *J. Am. Chem. Soc.*, 2007, **129**, 13402–13403; (b) P. A. Wender, A. B. Lesser and L. E. Sirois, *Angew. Chem., Int. Ed.*, 2012, **51**, 2736–2740.
- 19 K.-S. Masters, M. Wallesch and S. Bräse, *J. Org. Chem.*, 2011, **76**, 9060–9067.
- 20 U. Halbes-Letinois, J.-M. Weibel and P. Pale, *Chem. Soc. Rev.*, 2007, **36**, 759–769.
- 21 (a) C.-H. Lin, K.-H. Lin, B. Pal and L.-D. Tsou, *Chem. Commun.*, 2009, 803–805; (b) Y.-C. Lin, C.-H. Lin, C.-Y. Chen, S.-S. Sun and B. Pal, *Org. Biomol. Chem.*, 2011, **9**, 4507–4517.
- 22 S. Saito, S. Nobusue, E. Tsuzaka, C. Yuan, C. Mori, M. Hara, T. Seki, C. Camacho, S. Irle and S. Yamaguchi, *Nat. Commun.*, 2016, **7**, 12094–12100.
- 23 G. Angulo, M. Brucka, M. Gerecke, G. Grampp, D. Jeannerat, J. Milkiewicz, Y. Mitrev, C. Radzewicz, A. Rosspeintner, E. Vauthey and P. Wnuk, *Phys. Chem. Chem. Phys.*, 2016, **18**, 18460–18469.
- 24 (a) T. Yanai, D. P. Tew and N. C. Handy, *Chem. Phys. Lett.*, 2004, **393**, 51–57; (b) I. V. Rostov, R. Kobayashi and R. D. Amos, *Mol. Phys.*, 2012, **110**, 2329–2336.
- 25 S. Suzuki, S. Maeda and K. Morokuma, *J. Phys. Chem. A*, 2015, **119**, 11479–11487.
- 26 (a) L.-E. Salisbury, *J. Org. Chem.*, 1978, **43**, 4987–4991; (b) L.-E. Salisbury, *J. Org. Chem.*, 1978, **43**, 4991–4995; (c) G. Li, H. Fang, S. Zhang and Z. Xi, *Tetrahedron Lett.*, 2004, **45**, 8399–8402.
- 27 D. Shukla and P. Wan, *J. Am. Chem. Soc.*, 1993, **115**, 2990–2991.
- 28 M. Rosenberg, C. Dahlstrand, K. Kilså and H. Ottosson, *Chem. Rev.*, 2014, **114**, 5379–5425.
- 29 D. Jacquemin, *J. Chem. Theory Comput.*, 2016, **12**, 3993–4003.
- 30 (a) H. Watanabe, *Prog. Polym. Sci.*, 1999, **24**, 1253–1403; (b) W. W. Graessley, *J. Chem. Phys.*, 1967, **47**, 1942–1953.